AN EXPERIMENTAL STUDY ON ADDED MASS COEFFICIENT OF VORTEX-INDUCED VIBRATION OF A CIRCULAR CYLINDER

Reference NO. IJME 817, DOI: 10.5750/ijme.v164iA4.817

L Gao, China University of Petroleum, Beijing, China; CNOOC Research Institute, China, **J Gu, J Jia, L Chen, S Wang, C Huang,** College of Mechanical and Transportation Engineering, China University of Petroleum, Beijing, China

KEY DATES: Submitted: 08/12/21; Final acceptance: 22/02/23; Published: 27/03/23

SUMMARY

In this paper, an experiment study with aspect ratio 100 of a circular cylinder was conducted in a wave-current channel. The FBG sensors were attached on the circular cylinder which are used to capture vibration signal, two high-precision bellows type sensors were used to monitor fluctuant support force, and the dynamic response of circular cylinder was finally calculated by modal analysis method. The effect of flow velocity, mass ratio and top tension of circular cylinder on the amplitude ratio, frequency ratio and added mass coefficient was evaluated. The results showed that top tension had a greater influence on the amplitude; the added mass coefficient demonstrated a nonlinear relationship with external flow velocity. The added mass coefficient decreases when the reduced velocity increases. At a particular reduced velocity, the added mass coefficient decreases when the top tension increases or mass ratio increases.

KEYWORDS

Vortex-induced vibration; Experimental study; Top tension; Added mass coefficient

NOMENCLATURE

L	Total length (m)
D	Outer diameter (m)
L_s	Submerged Length (m)
m_0	Riser model weight (g)
EI	Bending stiffness (Nm2)
T	Top Tension (N)
V	Flow velocity (m/s)
Ur	Reduced velocity (-)
Re	Reynolds number (-)
P_e	Fiber's valid elastic-optic constants (-)
f_s	Sample rate (Hz)
n_{eff}	The effective refractive (-)
B_{ij}	Material strain tensor (-)
P_{11}	The elastic coefficients of the fiber (-)
P_{12}	The elastic coefficients of the fiber (-)
P_{44}	The elastic coefficients of the fiber (-)
v	Poisson's ratio(-)
m	The mass of a cylinder per unit length (g)
c	Structural damping (N.s/m)
k_{tot}	Structural stiffness (-)
m_a	Added mass (g)
Λ	Aspect ratio (-)
ε	Error of load cell (-)
$\lambda_{B\varepsilon}$	The center wavelength (m)
ε_{ij}	Strain coefficient (-)
ε_z	Axial strain (-)

1. INTRODUCTION

Vortex-induced vibration (VIV) usually occurs around the marine riser under the influence of external flow, which may cause marine riser fatigue. To avoid the damage caused by VIV, several prediction methods may be used. Usually, these methods are categorized as Semi-empirical method and Computational Fluid Dynamics (CFD). A comparison between laboratory measurements and blind predictions of eleven different numerical models was carried out by Chaplin *et al*. (2005a) to analyse the capability of different numerical tools to predict VIV (Chaplin, 2005). The Semi-empirical methods normally use the hydrodynamic force coefficients as a database, such as drag coefficient, lift coefficient, added mass coefficient and hydrodynamic damping coefficient. These coefficients are obtained from rigid cylinder model tests with forced motions.

For the added mass coefficient, it is usually set as constant during the numerical simulation (Facchinetti *et al*, 2004; Gu *et al*., 2012; Gu *et al*., 2013; Li *et al*., 2010; Srinil, 2011; Violette *et al*., 2007; Violette *et al*., 2007). However, Xu *et al*. (2008) conducted an experiment to reveal that the added mass coefficient decreases monotonically with reduced velocity (Vikestad *et al*., 2000). Clarke implemented Schwarz-Christoffel methods to calculate the added mass of elliptical and circular cylinders in shallow water (Clarke *et al*., 2001a; Clarke *et al*., 2001b). Then, Zhou *et al*. evaluated the effect of shallow and narrow water on added mass of cylinders with various cross-sectional shapes (Zhou *et al*., 2005).

Song *et al*. investigated hydrodynamic coefficients in both inline (IL) and cross-flow (CF) directions on flexible risers and found that the added-mass coefficient has a significant variation compared with that of a rigid cylinder oscillating in a pure CF or IL direction (Song *et al*., 2016). Song *et al*. developed an alternative time domain VIV force-decomposition model for flexible risers by considering added mass variation as a time varying function of response frequency (Zhou *et al*., 2005).

In recent years, scholars have used experimental methods to study the vortex-induced force parameters of the vortex-induced vibration of the riser, such as the added mass coefficient. Huera-Huarte *et al*. (2006) used the strain information in the CF and IL directions of the riser model obtained in the experiment to obtain the effect on the CF and IL directions. However, it did not further obtain the added mass coefficient in the CF and IL directions of the riser. Ren *et al*. (2020) obtained the damping coefficient and added mass coefficient of the vortex-induced vibration of the flexible pipe under the condition of oscillating flow by the experimental method. Aronsen *et al*. (2007) measured the fluid force of the rigid cylinder under pure co-current forced vibration and plotted the IL pulsation resistance coefficient and additional mass coefficient cloud diagram. However, they have little research on the relationship between the added mass coefficient of the riser and the flow rate, top tension, and mass ratio. Hence, to address the lack of study in ocean engineering, an experimental study on added mass coefficient of vortex-induced vibration of a circular cylinder is investigated. The present study is organized as follows. In the next section, the experiment set-up, parameters, and principle are presented initially. In the following section, the results and discussion including the time history of displacement, vibration mode, trajectories, amplitude and added mass coefficient are demonstrated. Finally, the study ends in last section with conclusions and perspectives.

2. EXPERIMENTAL DETAILS

2.1 EXPERIMENTAL SET-UP

The experiments were carried out in a cycling tank which has a test section 1.5 m in width, 1.5 m in height and 46 m in length, at the Key Laboratory of Marine Engineering of China National Petroleum Corporation (CNPC), Tianjin, China. The uniform flow was simulated by the cycling system. The experiments were repeated 3 times for each combination of flow velocity and top tension. Then the data were analyzed and revealed a high degree of repeatability. The current velocity ranges from 0.1 to 0.6 m/s, with approximate increments of 0.05 m/s. This range of velocity corresponds to Reynolds numbers from 1193 to 7160.

The sketch of the experimental set-up is shown in Fig. 1. The flexible cylinder had an outer diameter of 12 mm and was constructed of glass reinforced plastic tube. The instrumented flexible cylinder was pinned at both ends with two fisheye bearing so the flexible cylinder could oscillate in both IL direction and CF direction. The effective cylinder length was 1.2 m, with 0.48 m below water surface. The water coverage was 40% and therefore drag and lift forces could not be exerted on the full length of the cylinder. However, it has been verified by Chaplin *et al*. (2005b) that when a water coverage is higher than a threshold of 30%, the excited modes in the response will not change (Chaplin *et al*., 2005b). Additionally, a similar set-up has been used in the literatures (Huera-Huarte *et al*, 2009a; Huera-Huarte *et al*., 2009b; Huera-Huarte *et al*., 2011; Huera-Huarte *et al*., 2011).

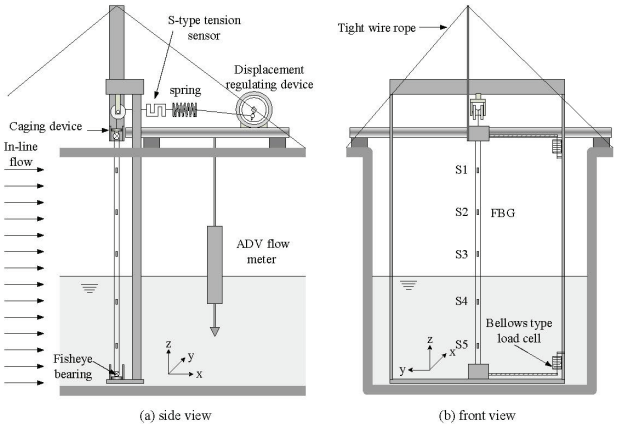

Figure 1. Sketch of the experiment set-up. (a) side view; (b) front view.

Fiber Bragg Grating (FBG) sensors are mounted on the flexible cylinder to measure the responses at five locations (identified as S1, S2, S3, S4 and S5), with the relative positions 0.84, 0.67, 0.50, 0.33, and 0.16 in length from the bottom end, respectively. At each location, two FBG sensors were placed in the x and y directions to measure the IL and CF vibrations. Two bellows type load cells are placed at each end to extract the supporting force of the circular cylinder.

The natural frequency of the circular cylinder with variable top tension was measured from plunk tests in still water. To find the experimental natural frequencies, the cylinder model was excited at its middle span after setting each different top tension. Table 1 shows the fundamental natural frequencies in term of different applied top tension.

Table 1: Fundamental natural frequencies at different applied top tension (Hz).

Top tension T(N)	M^*=2.38	M^*=2.97
0	3.40	3.86
10	3.87	4.35
20	4.21	4.70
30	4.70	5.00
40	5.90	6.70
50	6.19	7.00

The summary of the experiments showed in Table 2. The mass ratio is defined as $M^* = m_0/m_a$, m_0 denotes the cylinder model mass, *ma* denotes added mass; aspect ratio is defined as L/D; reduced velocity is defined as $Ur = V/f_0D$, V denotes the flow velocity, where f_0 is the natural frequency of the first mode; Reynolds number is defined as $\mathrm{Re} = \rho VD/\mu$, ρ and μ denote density and viscosity of the flow which were corrected for temperature.

Table 2: Summary of main parameters of the experiment.

Experiment parameters	Symbol	Unit	Value
Total length	L	m	1.2
Outer diameter	D	m	0.012
Submerged Length	L_s	m	0.48
Riser model weight	m_0	g	74
Bending stiffness	EI	Nm^2	2.06
Aspect ratio	Λ	-	100
Top Tension	T	N	0-50
Flow velocity	V	m/s	0.1-0.6
Reduced velocity	U_r	-	2-15
Reynolds number	Re	-	1193-7160
Error of load cell	ε	-	±0.02%
Fiber's valid elastic-optic constants	P_e	-	0.22
Sample rate	f_s	H_z	200

2.2 EXPERIMENTAL PRINCIPLE

The principle of FBG sensors is that the change of the strain causes the change of the reflected wavelength. By using the wavelength division multiplexing technology, multiple gratings can be connected (or burned) on one optical fiber to realize multi-point measurement. The center wavelength of the FBG is $\lambda_{B\varepsilon}$:

$$\lambda_{B\varepsilon} = 2n_{eff}\Lambda \tag{1}$$

where, n_{eff} denotes the effective refractive index of the light in the core of FBG; Λ is grating period. During the experiment, the water temperature in the water tank is controlled to be constant, and the deformation of the grating under the impact of the water flow causes the change of grating wavelength, so that the amount of change in wavelength can be expressed as:

$$\Delta\lambda_{B\varepsilon} = 2\Lambda\Delta n_{eff} + 2n_{eff}\Delta\Lambda \tag{2}$$

The axial strain of the grating can be expressed as (Hill *et al*., 1990)

$$\varepsilon_z = \Delta L / L = \Delta\Lambda / \Lambda \tag{3}$$

where ε_z is the axial strain of the grating, ΔL is the axial elongation and L is the length of the cylinder. By using the relationship

$$B_{ij} = 1/\varepsilon_{ij} = 1/n_{eff}^2 \tag{4}$$

between material strain tensor B_{ij} and strain coefficient ε_{ij}, derivation on both sides:

$$\Delta n_{eff} = -\Delta B_{ij} n_{eff}^3 / 2 \tag{5}$$

The following relationship can be obtained from equations 1-4:

$$\Delta\lambda_{B\varepsilon} = 2\Lambda[-\frac{n_{eff}^3}{2}\cdot\Delta(\frac{1}{n_{eff}^2})] + 2n_{eff}\Lambda\cdot\varepsilon_z \tag{6}$$

The elastic properties of the material have the following relationship:

$$\begin{bmatrix}\Delta B_1\\ \Delta B_2\\ \Delta B_3\\ \Delta B_4\\ \Delta B_5\\ \Delta B_6\end{bmatrix} = \begin{bmatrix}P_{11} & P_{12} & P_{12} & 0 & 0 & 0\\ P_{12} & P_{11} & P_{12} & 0 & 0 & 0\\ P_{12} & P_{12} & P_{11} & 0 & 0 & 0\\ 0 & 0 & 0 & P_{44} & 0 & 0\\ 0 & 0 & 0 & 0 & P_{44} & 0\\ 0 & 0 & 0 & 0 & 0 & P_{44}\end{bmatrix}\begin{bmatrix}\varepsilon_1\\ \varepsilon_2\\ \varepsilon_3\\ 0\\ 0\\ 0\end{bmatrix} \tag{7}$$

In the formula, ΔB_i is the change of tensor, P_{11}, P_{12} and P_{44} are the elastic coefficients of the fiber, and they have the relationship $P_{44} = (P_{11} - P_{12})/2$. Since the shear strain is zero, the strain tensor can be expressed as axial strain ε_z:

$$\varepsilon_j = \begin{bmatrix}-v\varepsilon_z & -v\varepsilon_z & \varepsilon_z & 0 & 0 & 0\end{bmatrix} \tag{8}$$

where v is the Poisson's ratio. The relative change in grating wavelength is:

$$\Delta\lambda_{B\varepsilon} / \lambda_{B\varepsilon} = (1 - P_e)\cdot\varepsilon_z \tag{9}$$

where effective elastic coefficient *Pe* is:

$$P_e = \frac{1}{2}n_{eff}^2[P_{12} - v(P_{11} + P_{12})] \tag{10}$$

In present experiment, the effective elastic coefficient of the erbium-doped quartz fiber used is 0.22, then formula (9) can be written as:

$$\Delta\lambda_{B\varepsilon} / \lambda_{B\varepsilon} = 0.78\cdot\varepsilon_z \tag{11}$$

According to the theory of plane hypothesis and the relationship between strain and curvature in elastic mechanics, the curvature of the circular cylinder is:

$$\kappa(z,t) = y''(z,t) = \frac{2\times\varepsilon(z,t)}{D} \tag{12}$$

The two ends of the circular cylinder are connected by fisheye bearings, and the mode shape function can be expressed as (Gu *et al*., 2012) [6]:

$$\varphi_n(z) = \sin\frac{n\pi z}{L} \tag{13}$$

The curvature of each mode of the cylinder is:

$$\theta_n(z) = \frac{d^2\varphi_n(z)}{dz^2} \tag{14}$$

The curvature of the circular cylinder can be expressed in the form of modal decomposition (Lie and Kaasen, 2006) [14]:

$$\kappa(z,t) = \sum_{n=1}^{\infty} w_n(t)\theta_n(z) \approx -(\frac{n\pi}{L})^2 \sum_{n=1}^{\infty} w_n(t)\varphi_n(z) \tag{15}$$

where *wn* denotes the weight of each mode. The curvature can be measured according to the grating sensor arranged on the circular cylinder, and five FBGs are arranged in a single direction of circular cylinder. Assuming that the maximum mode number which the flow velocity can excite is *N*, the parts in equation (15) are written in the form of vectors:

$$\begin{cases} \theta_n = [\theta_n(z_1), \theta_n(z_2), ..., \theta_n(z_5)]^T \\ \Theta = [\theta_1, \theta_2, ..., \theta_N] \\ \kappa(t) = [\kappa_1(t), \kappa_2(t), ..., \kappa_M(t)]^T \\ w(t) = [w_1(t), w_2(t), ..., w_M(t)]^T \\ where\ n = 1, 2, ..., N \end{cases} \tag{16}$$

Then formula (14) can be expressed as:

$$\kappa(t) = \Theta w(t) \tag{17}$$

When the mode number in which the cylinder is excited and the number of gratings are not equal, the weight coefficient can be expressed as:

$$w(t) = (\Theta^T\Theta)^{-1}\Theta^T\kappa(t) \tag{18}$$

The governing equation of the circular cylinder can be expressed as (Vikestad *et al*., 2000) [17]

$$m\ddot{y} + c\dot{y} + k_{tot}y = F_v(t) \tag{19}$$

For the solution of the added mass coefficient, the integral method proposed by Vikestad *et al*. (2000) [17] can be expressed as:

$$C_a = \frac{m_a}{m_0} = -\lim_{T\to\infty} \frac{2}{m_0 T(\omega^2 y_0)^2} \int_t^{t+T} F_v \ddot{y} dt \tag{20}$$

where $F_v(t)$ is the hydrodynamic force for the cross flow, m_0 is the mass of the circular cylinder in the still water, and T is the period of the vibration, w is the circular frequency of the vibration. The weight of each mode is extracted by the modal analysis from formula (18), and then the vibration shape of the circular cylinder is determined. The added mass coefficient is obtained by using the formula (20).

3. RESULTS AND DISCUSSION

To study the natural frequency of the riser under different mass ratios, steel balls with diameters of 5mm and 2mm were added into the riser successively in the experiment, so that the mass ratios of the riser in water were 2.38 and 2.97. It can be seen from Table 1 that the natural frequency of the riser increases with the increase of the top tension when the mass ratio is unchanged. Under the condition of constant top tension, the natural frequency of the riser increases with the increase of the riser mass ratio. It is obvious that the riser frequency increases most sharply at the top tension of 30N to 40N.

Fig. 2 and Fig. 3 show the typical CF and IL time histories and the response frequencies respectively, at T = 0 N, V = 0.30 m/s, M^* = 2.38. The first column graph shows the time history of CF displacement in diameter for a complete run at each station of FGB sensors along the cylinder in a time interval $t \in$ [5,15] s. The second column graph shows the time history in a time interval $t \in$ [9,11] s. The third column graph shows the spectral analysis of each signal without mean. The second column graph demonstrates a stable instantaneous displacement. As shown in the third column, only one peak of vibration frequency appeared in the CF spectral analysis, whereas two peaks are captured in the IL spectral analysis. This phenomenon reveals that the IL vibration captured the second mode, and the vibration frequency of the first mode should be influenced by the CF vibration.

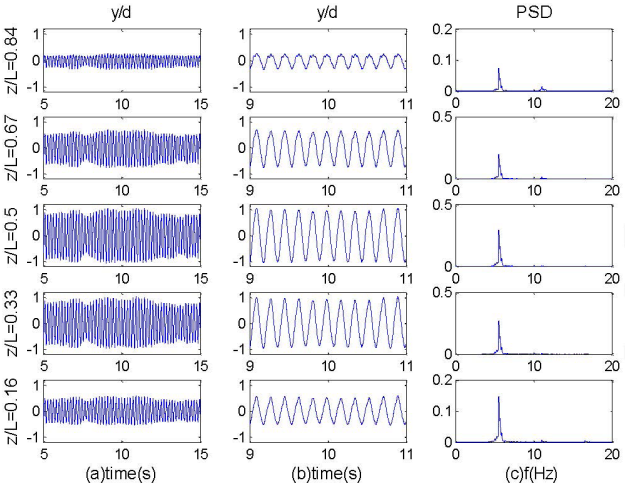

Figure 2. Time history of test at T = 0 N, V = 0.3 m/s, M^* = 2.38. (a) Time history of CF displacement in an interval $t \in$ [5,15] s, (b) Time history in an interval $t \in$ [9,11] s, (c) Spectral analysis of each signal without mean.

The modal analysis method is used to obtain the weights of each mode, and the inverse transform is performed to get the instantaneous vibration shapes. The vibration shapes are decomposed into the first three mode shapes according to the weight as shown Fig. 4 at mass ratio M^* = 2.38, top tension T = 20N, flow velocity v = 0.4 m/s. The left side of the figure shows the instantaneous vibration shapes of the first three modes in CF direction, and the right side shows the ones in IL direction. It can be noted that the first mode is dominated in the vibration in both CF and IL

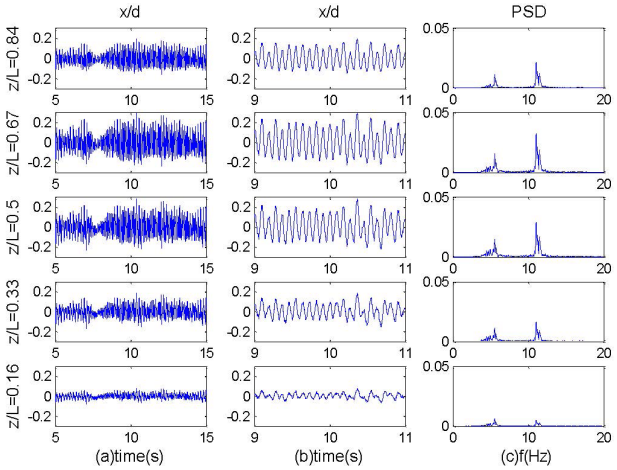

Figure 3. Time history of test at $T = 0$ N, $V = 0.3$ m/s, $M^* = 2.38$. (a) Time history of IL displacement in an interval $t \in$ [5,15] s, (b) Time history in an interval $t \in$ [9,11] s, (c) Spectral analysis of each signal without mean.

directions, the contribution of the second mode is less than the first, and the third mode almost has no contribution to the overall response.

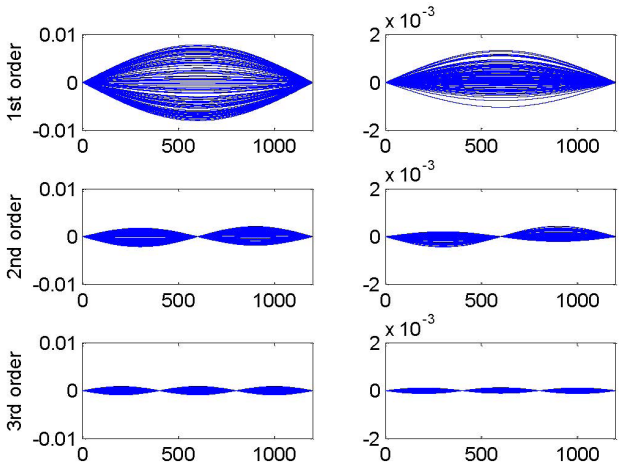

Figure 4. The component decomposition of modal weights: CF (left) and IL (right) oscillations up to the third mode when $T = 20$ N, $V = 0.4$ m/s, $M^* = 2.38$.

Fig. 5 shows the instantaneous x − y trajectories versus flow velocity at each FBG sensor station at mass ratio $M^* = 2.38$, top tension $T = 0$N. The cases of $V = 0.3$ and $V = 0.35$ are clearly exhibited a figure-8 pattern at $z/D = 0.67, 0.5, 0.33$. Fig. 6 presents the vibration amplitude with respect to the reduced velocity. Since the points at each reduced velocity is not continuous, a cure fit is conducted. It can be seen from the figure that the curves have upper and lower branches. For instance, the amplitude ratio A/D increases rapidly in the interval [4,7], and a rapid decrease in the interval [7,9] at $T = 30$N. When the reduced velocity is greater than 10, the curve shows a tendency of slow growth, and it can be inferred that higher flow vibrations may be excited when the flow velocity is increased.

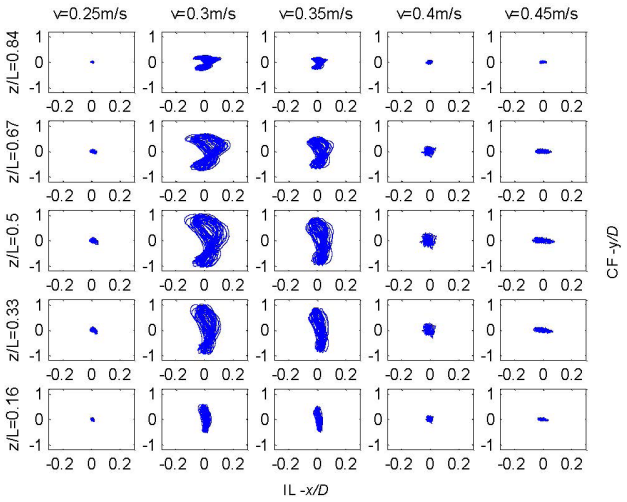

Figure 5. In-line and cross-flow trajectories at different velocities when $T = 0$ N, $M^* = 2.38$.

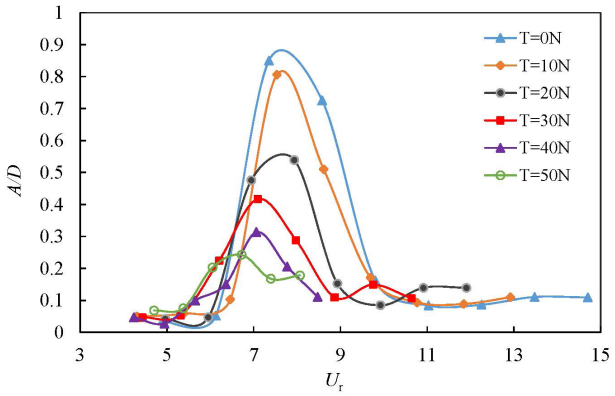

Figure 6. Vibration amplitude versus reduced velocity at various top tension.

The ratio between the CF vibration frequency and natural frequency of the circular cylinder versus reduced velocity is depicted in Fig. 7. Two lines are clearly presented, and one of them appears horizontal red line with a value of 1.2, which is greater than 1. The reason is that the natural frequency of the circular cylinder increases as the added mass coefficient decreases in the resonance region, and the vibration frequency is locked with the new natural frequency. Then the calculation of frequency ratio f/f_0 will be greater than one in which the f_0 is the initial natural frequency. When the cylinder vibration is out of the locked zone, its vibration frequency will increase when the flow velocity increases, showing a linear relationship as presented by the black line in the figure. It can also be noted that the top tension has little effect on the vibration frequency ratio.

The integration method is used to obtain a relationship between the added mass coefficient and the reduced velocity, as shown in Fig. 8. The added mass coefficient decreases as the reduced velocity increases, and it gradually approaches to -1. When the reduced velocity is less than 8, it can be clearly seen that the increase of the top tension

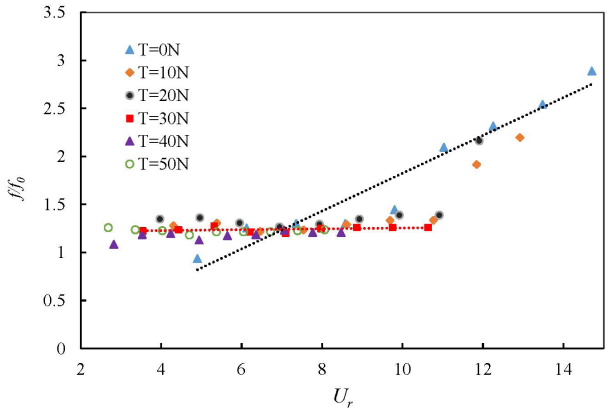

Figure 7. Frequency ratio versus reduced velocity at various top tension.

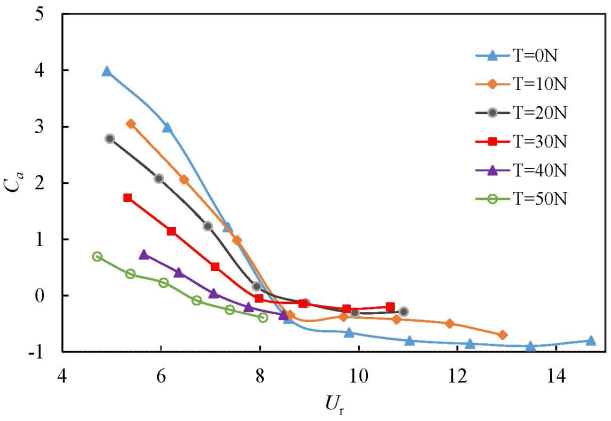

Figure 8. Added mass coefficient versus reduced velocity at various top tension.

will induce the decrease of the slope of the added mass coefficient curve. In another words, at a particular reduced velocity, the added mass coefficient decreases as the top tension increases.

Two different mass ratios of circular cylinder are studied during the experiment, and the added mass coefficients versus reduced velocity are plotted in Fig. 9 when $T = 30$N. From the figure, it is found that the increase of the mass ratio will induce the added mass coefficient curve moving to the left. For example, when the mass ratio $M^* = 2.38$, the zero point appears between $U_r \in [6,7]$; when the mass ratio $M^* = 2.97$, the zero point appears between $U_r \in [8; 9]$. Therefore, it is inferred that the larger the mass ratio, the smaller the zero point of the curve. Meanwhile, at a particular reduced velocity, the increase of mass ratio will induce the decrease of the added mass coefficient.

The direct relationship between the top tension and circular cylinder response is specific for each application. As shown in Fig. 8, when the reduced velocity is in the range of 4 to 7, the higher the top tension is, the smaller the added mass coefficient of the circular cylinder is. However, when the reduced velocity is in the range of 10 to 11, the added mass coefficient of the circular cylinder increases with the increase of the top tension. Beam theory is used to simulate the

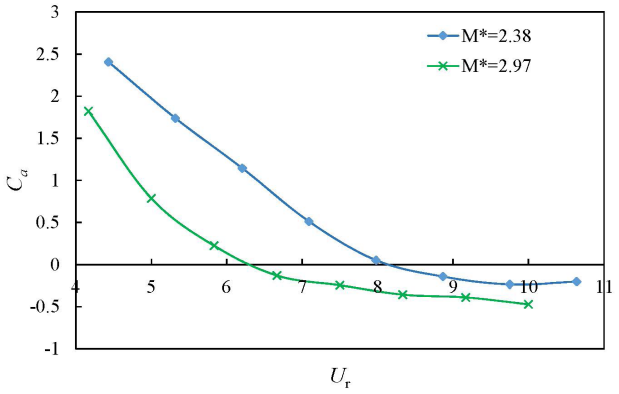

Figure 9. Added mass coefficient versus reduced velocity at $M^* = 2.38$ and $M^* = 2.97$.

characteristics of vibration of the circular cylinder, the natural frequency of vibration of the circular cylinder formula is:

$$f = \frac{(i\pi)^2}{2\pi L^2}\left(1+\frac{PL^2}{(i\pi)^2 EI}\right)^{1/2}\left(\frac{EI}{m}\right)^{1/2} \tag{20}$$

As shown in Equation (20), when the top tension is greater than 0N, the natural frequency of the circular cylinder increases with the value of the top tension. When the top tension is less then 0N, the natural frequency of the circular cylinder decreases with the increase of the top tension.

The uncertainty analysis of the additional mass factor can be obtained from Equation (19). The influencing parameters of the additional mass factor are the mass-related cylinder diameter and length, the top tension, the riser mass, and the hydrodynamic component in the CF direction. For diameter and length measurements of risers, use vernier caliper to measure the diameter of the cylinder at random locations and take multiple readings, use a tape measure to measure the length of the cylinder multiple times, and then take the average to calculate their error from the standard value. The top tension of the cylinder is measured several times using a force sensor. Due to the installation of the test device, there is an inevitable angle error between the riser and the direction of the water flow, resulting in a deviation of the hydrodynamic force F_v on the riser. Their deviations are shown in Table 3, and the values in parentheses are the ratios of the deviations produced by the measured data to the standard values. The deviations of all parameters are less than 1%, among which the deviation of the top tension and the hydrodynamic component in the CF direction is larger.

Table 3: Additional mass coefficient parameter deviation.

Parameter	Deviation
D	0.012mm（0.1%）
L	2mm（0.02%）
T	0.2N（0.2%）
m_0	0.1g(0.1%)
F_v	0.2N（0.2%）

4. CONCLUSIONS

An experimental study is conducted to evaluate the effects of top tension and mass ratio on the added mass coefficient of the circular cylinder, and the following conclusions are drawn:

(i) The added mass coefficient decreases when the reduced velocity increases;

(ii) At a particular reduced velocity, the added mass coefficient decreases when the top tension increases;

(iii) At a particular reduced velocity, the added mass coefficient decreases when the mass ratio increases.

This investigation verifies that the added mass coefficient do have relationship with the flow velocity, top tension and mass ratio, and it is suggested that these should be considered in the prediction model of vortex-induced vibration of slender structures, such as jumpers, risers and subsea pipelines.

5. ACKNOWLEDGEMENTS

The authors acknowledge gratefully the financial support provided by the Science Foundation of China University of Petroleum, Beijing (Grant Nos. 2462020YXZZ046), the China National Key Research and Development Plan (Grant Nos. 2017YFC0805803) for the financial support of this research.

6. REFERENCES

1. CHAPLIN, J. R., BEARMAN, P. W., CHENG, Y., FONTAINE, E., GRAHAM, J. M. R., HHERFJORD, K., HUERA-HUARTE, F. J., ISHERWOOD, M., LAMBRAKOS, K., LARSEN, C. M., MENEGHINI, J. R., MOE, G., PATTENDEN, R., TRIANTAFYLLO, M. S., WILLDEN, R. H. J., 2005a. *Blind predictions of laboratory measurements of vortex-induced vibrations of a tension riser*. Journal of Fluids and Structures 21 (1), 25-40. DOI: 10.1016/j.jfluidstructs.2005.05.016
2. CHAPLIN, J. R., BEARMAN, P. W., HUERA-HUARTE, F. J., PATTENDEN, R. J., 2005b. *Laboratory measurements of vortex-induced vibrations of a vertical tension riser in a stepped current.* Journal of Fluids and Structures 21 (1), 3-24. DOI: 10.1016/j.jfluidstructs.2005.04.010
3. CLARKE, D., 2001a. *Calculation of the added mass of circular cylinders in shallow water.* Ocean Engineering 28 (9), 1265-1294. DOI: 10.1016/S0029-8018(00)00064-0
4. CLARKE, D., 2001b. *Calculation of the added mass of elliptical cylinders in shallow water.* Ocean Engineering 28 (10), 1361-1381. DOI: 10.1016/S0029-8018(00)00054-8
5. FACCHINETTI, M. L., DE LANGRE, E., BIOLLEY, F., 2004. *Coupling of structure and wake oscillators in vortex-induced vibrations.* Journal of Fluids and Structures 19 (2), 123-140. DOI: 10.1016/j.jfluidstructs.2003.12.004
6. GU, J., AN, C., LEVI, C., SU, J., 2012. *Prediction of vortex-induced vibration of long flexible cylinders modeled by a coupled nonlinear oscillator: Integral transform solution.* Journal of Hydrodynamics, Ser. B 24 (6), 888-898. DOI: 10.1016/S1001-6058(11)60317-X
7. GU, J., WANG, Y., ZHANG, Y., DUAN, M., LEVI, C., 2013. *Analytical solution of mean top tension of long flexible riser in modeling vortex-induced vibrations.* Applied Ocean Research 41, 1-8. DOI: 10.1016/j.apor.2013.01.004
8. HILL, K. O., MALO, B., VINEBERG, K. A., BILODEAU, F., 1990. *Efficient mode conversion in telecommunication fibre using externally written gratings.* Electronics Letters 26 (16), 1270-1272. DOI: 10.1049/el:19900818
9. HUERA-HUARTE, F. J., BEARMAN, P. W., 2009a. *Wake structures and vortexinduced vibrations of along flexible cylinder-part 1: Dynamic response.* Journal of Fluids and Structures 25 (6), 969-990. DOI: 10.1016/j.jfluidstructs.2009.03.007
10. HUERA-HUARTE, F. J., BEARMAN, P. W., 2009b. *Wake structures and vortex-induced vibrations of along flexible cylinder-part 2: Drag coefficients and vortex modes.* Journal of Fluids and Structures 25 (6), 991-1006. DOI: 10.1016/j.jfluidstructs.2009.03.006
11. HUERA-HUARTE, F. J., BEARMAN, P. W., 2011. *Vortex and wake-induced vibrations of a tandem arrangement of two flexible circular cylinders with near wake interference.* Journal of Fluids and Structures 27 (2), 193-211. DOI: 10.1016/j.jfluidstructs.2010.11.004
12. HUERA-HUARTE, F. J., GHARIB, M., 2011. *Flow-induced vibrations of a side-byside arrangement of two flexible circular cylinders.* Journal of Fluids and Structures 27 (3), 354-366. DOI: 10.1016/j.jfluidstructs.2011.01.001
13. LI, X.-M., GUO, H.-Y., MENG, F.-s., 2010. *Nonlinear coupled in-line and crossflow vortex-induced vibration analysis of top tensioned riser.* China Ocean Engineering 4, 749-758.
14. LIE, H., KAASEN, K. E., 2006. *Modal analysis of measurements from a largescale viv model test of a riser in linearly sheared flow.* Journal of Fluids and Structures 22 (4), 557-575. DOI: 10.1016/j.jfluidstructs.2006.01.002
15. SONG, L., FU, S., ZENG, Y., CHEN, Y., 2016. *Hydrodynamic forces and coefficients on flexible risers undergoing vortex-induced vibrations in*

uniform flow. Journal of Waterway Port Coastal & Ocean Engineering 142 (4), 04016001. DOI: 10.1061/(ASCE)WW.1943-5460.0000333

16. SRINIL, N., 2011. *Analysis and prediction of vortex-induced vibrations of variable-tension vertical risers in linearly sheared currents.* Applied Ocean Research 33 (1), 41-53. DOI: 10.1016/j.apor.2010.11.004
17. VIKESTAD, K., VANDIVER, J. K., LARSEN, C. M., 2000. *Added mass and oscillation frequency for a circular cylinder subjected to vortex-induced vibrations and external disturbance*. Journal of Fluids and Structures 14 (7), 1071-1088. DOI: 10.1006/jfls.2000.0308
18. VIOLETTE, R., DE LANGRE, E., SZYDLOWSKI, J., 2007. *Computation of vortexinduced vibrations of long structures using a wake oscillator model: Comparison with DNS and experiments.* Computers & Structures 85 (11-14), 1134-1141. DOI: 10.1016/j.compstruc.2006.08.005
19. XU, W.-H., ZENG, X.-H., WU, Y.-X., 2008. *High aspect ratio (l/d) riser viv prediction using wake oscillator model.* Ocean Engineering 35 (17-18), 1769-1774. DOI: 10.1016/j.oceaneng.2008.08.015
20. YUAN, Y.-C., E, H.-X., TANG, W.-Y., 2018. *Added mass variation effect on vortex-induced vibration for flexible risers based on force-decomposition model*. Ships and Offshore Structures 13 (sup1), 1-12. DOI: 10.1080/17445302.2017.1416908
21. ZHOU, Z., LO, E. Y., TAN, S., 2005. *Effect of shallow and narrow water on added mass of cylinders with various cross-sectional shapes.* Ocean Engineering 32 (10), 1199 -1215. DOI: 10.1016/j.oceaneng.2004.12.001
22. HUERA-HUARTE FJ, BEARMAN PW, CHAPLIN JR (2006) *On the force distribution along the axis of a flexible circular cylinder undergoing multi-mode vortex-induced vibrations.* Journal of Fluids and Structures 22(6- 7): 897–903. DOI: 10.1016/j.jfluidstructs.2006.04.014
23. REN H, ZHANG M, WANG Y *et al*. (2020) *Drag and added mass coefficients of a flexible pipe undergoing vortex-induced vibration in an oscillatory flow*. Ocean Engineering 210(1): 107541 DOI: 10.1016/j.oceaneng.2020.107541
24. ARONSEN,K.H. *An experimental investigation of inline and combinedin-line and cross-flow vortex induced vibrations.* Ph.D. Thesis, Trondheim: Norwegian University of Science and Technology, 2007.